

PCCP

Accepted Manuscript



This is an *Accepted Manuscript*, which has been through the Royal Society of Chemistry peer review process and has been accepted for publication.

Accepted Manuscripts are published online shortly after acceptance, before technical editing, formatting and proof reading. Using this free service, authors can make their results available to the community, in citable form, before we publish the edited article. We will replace this *Accepted Manuscript* with the edited and formatted *Advance Article* as soon as it is available.

You can find more information about *Accepted Manuscripts* in the [Information for Authors](#).

Please note that technical editing may introduce minor changes to the text and/or graphics, which may alter content. The journal's standard [Terms & Conditions](#) and the [Ethical guidelines](#) still apply. In no event shall the Royal Society of Chemistry be held responsible for any errors or omissions in this *Accepted Manuscript* or any consequences arising from the use of any information it contains.

Identifying sp - sp^2 carbon materials by Raman and Infrared Spectroscopies

Cite this: DOI: 10.1039/x0xx00000x

Jinying Wang,^a Shuqing Zhang,^a Jingyuan Zhou, Rong Liu, Ran Du, Hua Xu, Zhongfan Liu,* Jin Zhang* and Zhirong Liu*

Received 00th January 2012,
Accepted 00th January 2012

DOI: 10.1039/x0xx00000x

www.rsc.org/

Two-dimensional (2D) materials composed of sp and sp^2 carbon atoms (e.g., graphyne and graphdiyne) show many interesting properties. These materials can be constructed through alkyne homocoupling; however, the occurrence of various side reactions increases the difficulty of their synthesis and structural characterization. Here, we investigate the thermodynamic properties and vibrational spectra of several aryl-alkynes. Both homocoupling and side reactions are found to occur spontaneously at room temperature in terms of thermodynamics. The calculated Raman spectra of the homocoupling products show regular changes with increasing polymerization degree. By rationalizing the vibrational modes of various oligomers, the Raman spectrum of a 2D sp - sp^2 carbon sheet is predicted; it exhibits three sharp peaks at 2241, 1560, and 1444 cm^{-1} . Although the target and byproducts display similar vibrational modes, a combination of Raman and infrared spectroscopies can be used to differentiate them. The theoretical results are then used to analyze the structure of a synthesized sample and provide useful information.

1. Introduction

Carbon forms various stable structures including diamond, graphite, fullerenes, carbon nanotubes (CNTs), and amorphous carbon materials. All of the existing and proposed carbon allotropes can be described as networks constructed from different combinations of sp^3 -, sp^2 - and sp -hybridized carbon atoms.¹ The discovery of graphene in 2004 and the numerous subsequent studies² have inspired the search for novel carbon allotropes.^{3–8} Among the multifarious predicted carbon allotropes, the graphyne family,^{9–10} which is a series of two-dimensional (2D) materials composed of sp and sp^2 carbon atoms, has received increasing attention because of the unique properties of its members.^{4,11–16} These new carbon forms can behave as both metallic and semiconductive materials,^{4,11} and Dirac cones have been found in some specific configurations.^{12,16} Theoretical studies have shown that sp - sp^2 carbon materials could possess excellent mechanical properties.^{13,15} Applications of sp - sp^2 carbon materials in electronic devices,¹⁷ gas separation,^{17–19} energy storage,^{20–22} catalysis,^{23–24} and solar cells²⁵ have been proposed.

Experimentally, the synthesis of infinite sp - sp^2 carbon materials is challenging and little success has been achieved. Initially, organic chemists only obtained oligomers.^{26–28} In 2010, Li *et al.*²⁹ fabricated large graphdiyne films *via* a homocoupling reaction on copper surfaces, representing an encouraging step towards synthetic 2D polymers. Because of the lack of single or few-layer samples, structural characterization of the obtained graphdiyne films is also difficult. Recent experiments have indicated that several coupling reactions of ethynyl groups tend

to occur simultaneously to form complex products.^{30–33} Therefore, the efficient characterization of sp - sp^2 carbon materials is an important goal.

Vibrational spectroscopy (Raman and infrared (IR)) is a popular and convenient tool to characterize carbon materials.^{34–35} Raman spectroscopy has been widely used to identify the layer number, defects and disorder, and doping level of graphene,^{36–37} as well as the diameter and chirality of CNTs.³⁸ Naturally, one may expect Raman spectroscopy to play an important role in the study of sp - sp^2 carbon materials. However, some basic vibrational properties of sp - sp^2 carbon materials remain unclear. For example, how do Raman spectra change with the degree of oligomerization? Can the homocoupling products be differentiated from others?

In this work, we conduct a theoretical and experimental study of the thermodynamic properties and vibrational spectra of several arylalkynes. This study has three objectives: to suggest how to promote the homocoupling of arylalkynes, to reveal how the Raman spectra of sp - sp^2 systems change with the degree of polymerization, and to demonstrate the usefulness of Raman and IR spectroscopies in identifying the various structures in these systems.

2. Theoretical and experimental methods

2.1 Density functional theory calculation

All calculations were performed using density functional theory (DFT) with the Gaussian 03 package.³⁹ For the thermodynamic analysis, the hybrid functional B3LYP with the

6-311+G(d,p) basis set was used because of its good performance in thermochemistry.⁴⁰ Geometric optimizations were carried out at the same level. A test of the calculation method is provided in **Table S1** in the Supporting Information. To calculate Raman and IR spectra, we chose the PBE functional and 6-311+G(d,p) basis set after a series of tests (see **Figure S1** and **S2** in the Supporting Information). The differences between the theoretical and experimental values of Raman peak positions for a few investigated compounds were less than 30 cm^{-1} in the range $1200\text{--}2400\text{ cm}^{-1}$, confirming the reliability of the calculations. To reveal the general trends of the Raman spectra with increasing degree of oligomerization in $sp\text{--}sp^2$ carbon materials, the Raman spectra of some large systems were also calculated with the 6-31G(d) basis set and PBE functional. The calculated vibrational frequencies were analyzed on the basis of potential energy distribution (PED) with the VEDA program,^{41,42} which has been successfully used to analyze the distribution of vibrational energy previously.^{43,44} With the help of VEDA, the assignment of bands was performed by internal coordinates.

2.2 Material synthesis and spectra measurements

Alkynes and solvents were obtained commercially and used without further purification. Copper foil was electrochemically polished in a phosphoric acid–glycol solution for 30 min, dried under a flow of nitrogen, and used immediately. 1,3,5-Triethynylbenzene (**1**, TEB, 0.015 g) was added to pyridine (100 mL) to prepare a solution with a concentration of 10^{-3} mol/L, and then a piece of copper foil ($1\text{ cm} \times 1\text{ cm}$) was added to 10 mL of this solution. The mixture was stirred at $50\text{ }^\circ\text{C}$ in an oil bath for 48 h. The copper foil was then washed sequentially with pyridine (20 mL) and dimethyl sulfoxide (20 mL) to remove monomers and oligomers. After drying the copper foil under a flow of nitrogen, a $sp\text{--}sp^2$ carbon film was obtained on the copper foil. Raman spectra were measured on a Horiba HR800 Raman spectrometer using a 632.8-nm excitation laser. Fourier transform IR spectra were recorded on a ThermoScientific Nicolet iN10 MX FT-IR spectrophotometer.

3. Results and discussion

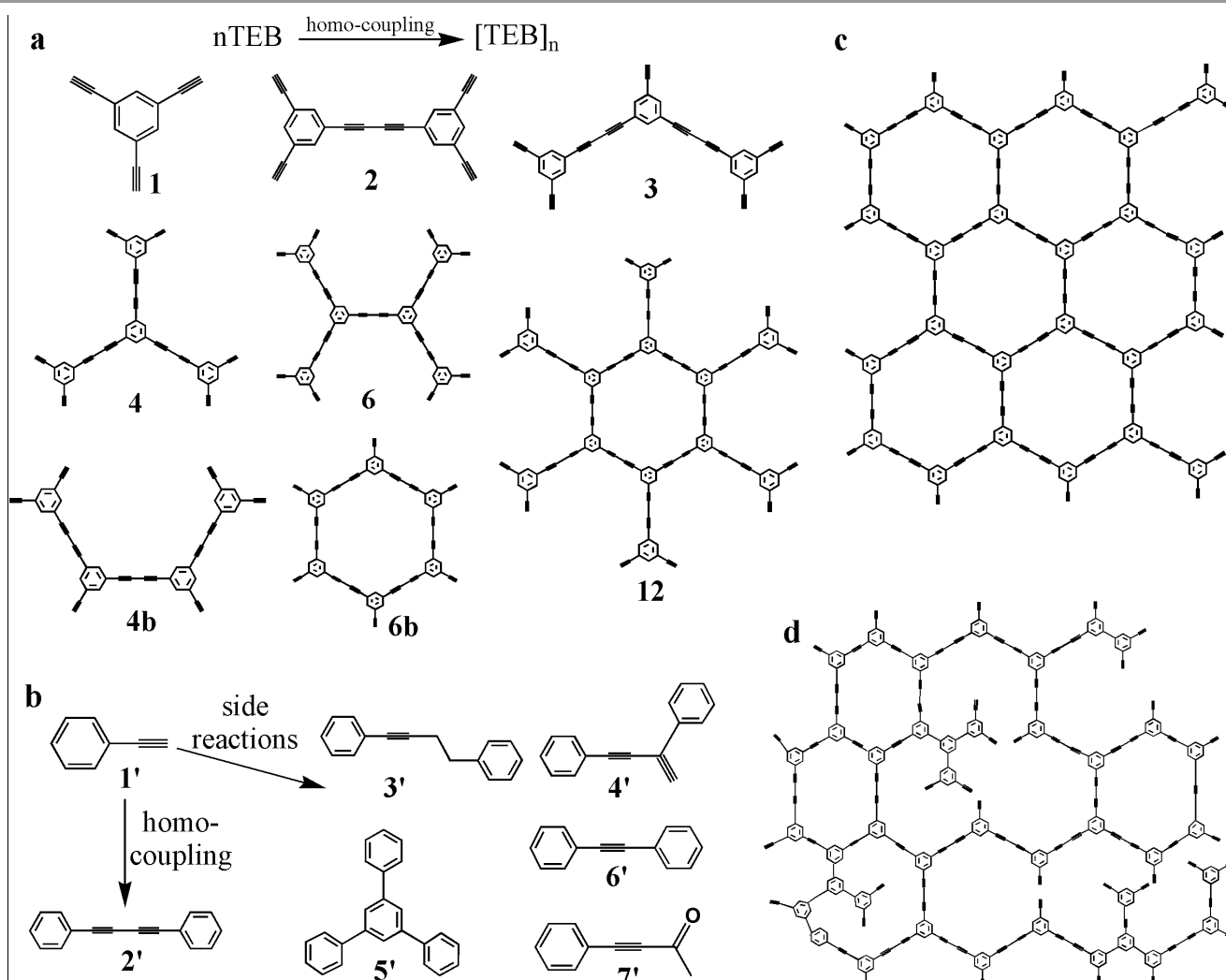


Figure 1. Reaction schemes and products. (a) Homocoupling of **1** (TEB) to produce oligomers **2**, **3**, **4**, **4b**, **6**, **6b**, and **12**. (b) **1'** (phenylacetylene, PA) and its homocoupling product **2'** and various byproducts **3'**–**7'**. (c) Ideal 2D crystal of polymerized **1**. (d) A hypothetical network with irregular crosslinked of **1**.

3.1 Thermodynamic properties

We used compound **1** (TEB, **Figure 1a**) as the monomer unit to construct the 2D sp–sp² carbon materials shown in **Figure 1c**. When a homocoupling reaction occurs, a C–C covalent bond forms between two ethynyl groups, so the TEB monomer **1** is transformed into dimers **2**, trimers **3**, tetramers **4**, and other oligomers **4b**, **6**, **6b**, **12** (**Figure 1a**), and then may be eventually transformed into a 2D material (**Figure 1c**). However, experiments in solution and under ultrahigh vacuum (UHV) have revealed that several types of side reactions can also occur, such as hydroalkynylation, trimerization, and oxidation,^{30–32} leading to the random polymeric networks depicted in **Figure 1d**. To investigate the various reaction pathways, we chose a simpler molecule **1'** (phenylacetylene, PA) as the reactant, from which molecules **2'–7'** were possible products (**Figure 1b**).

We first examined the thermodynamic properties of the homocoupling and side reactions (**Figure 2**). The change in standard enthalpy (ΔH_r) and Gibbs free energy (ΔG_r) for molecules in the gas phase were calculated by

$$\begin{aligned} \Delta H_r &= \sum H_{pr} - \sum H_{re} \\ \Delta G_r &= \sum G_{pr} - \sum G_{re} \end{aligned} \quad (1)$$

where H_{pr} (G_{pr}) is the enthalpy (Gibbs free energy) of the product and H_{re} (G_{re}) is that of the reactant. ΔH_r and ΔG_r for the monomers (compounds **1** and **1'**) were set to 0. The specific reaction pathways are summarized in **Figure 2a**. It should be noted that the homocoupling reactions might have two different pathways: (1) oxygen acts as an oxidant, which is the situation that usually occurs in solution; and (2) the C–C bonds form along with dehydrogenation (usually under UHV conditions).³¹

Figure 2b shows that all of the reactions are exothermic processes at room temperature. The difference between ΔH_r and ΔG_r is small, especially for the homocoupling reaction. For pathway (1) involving oxygen molecules (emphasized by red arrows in **Figure 2a**), ΔH_r and ΔG_r (red symbols in **Figure 2b**) are comparable with those of the side reactions (black symbols), and decrease with polymerization degree n . However, for pathway (2) including hydrogen generation (emphasized by blue arrows in **Figure 2a**), the corresponding ΔH_r and ΔG_r (blue symbols in **Figure 2b**) are very small (about -2 kcal/mol). This suggests that this type of reaction is relatively disadvantaged in thermodynamics. Previous studies have indicated that the substrates have the important effect of stabilizing 2D carbon materials. For example, the interaction between various metal substrates and graphene can decrease the

energy of systems by 0.1–0.9 eV.⁴⁵ The novel sp–sp² carbon allotrope graphdiyne has also been synthesized on metal surfaces.²⁸ Therefore, the introduction of oxygen and selection of an appropriate metal substrate might increase the tendency to form the target 2D materials.

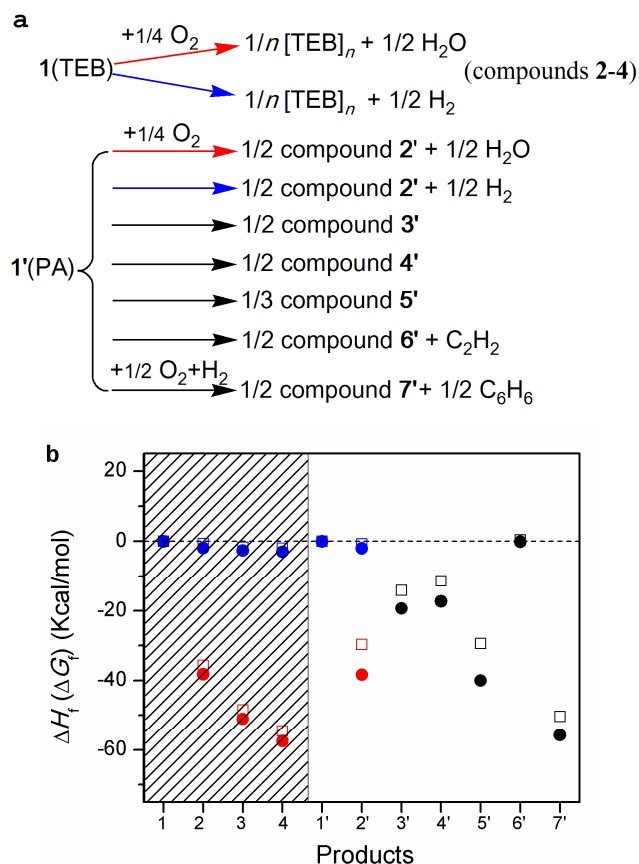


Figure 2. Reaction pathways and thermodynamic analysis. (a) Pathways of homocoupling with oxygen participating (red arrows), dehydrogenation (blue arrows), and side reactions (black arrows). [TEB]_n denotes the homocoupling products of TEB with polymerization degree n . (b) The changes of standard enthalpy ΔH_r are shown as solid circles and the Gibbs free energy ΔG_r as open squares. Red is used for the oxidative homocoupling pathway, blue for the pathway with dehydrogenation, and black for the side reactions.

3.2 Raman spectra of oligomers

The above thermodynamics calculations suggest that homocoupling of alkynes should proceed exothermically. In experiments, it is difficult to identify the degree and direction of polymerization. The vibrations of a molecule are closely related to its structures, so we calculated the Raman spectra of the TEB monomer **1** and its oligomers to investigate how the Raman spectra change with polymerization (**Figure 3**).

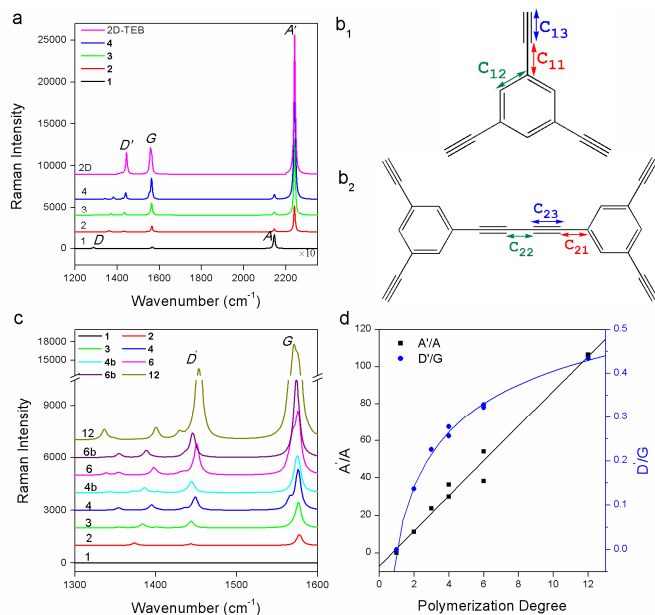


Figure 3. Calculated Raman spectra of the TEb monomer **1** and its oligomers, the intensity of peaks are expressed by the calculated amplitude. (a) Raman spectra of monomer **1** (the intensity has been amplified by 10), homocoupling oligomers **2**, **3**, **4**, and 2D TEb sheet. (b₁) Monomer **1**, where C₁₁, C₁₂, and C₁₃ represent the bonds between triply-coordinated atoms and its doubly-coordinated neighbors, the bonds of aromatic rings, the bonds of carbon triple bonds in TEb monomer, respectively. (b₂) Dimer **2**, where C₂₁, C₂₂, C₂₃ represent bonds between a triply-coordinated atoms and its doubly-coordinated neighbors, the single bonds between two triple carbon bonds, and the carbon triple bonds in TEb dimer, respectively. (c) Raman spectra of the systems **1–4**, **4b**, **6**, **6b**, and **12** calculated with the 6-31g(d) basis set. (d) Raman intensity ratios of A' to A (A'/A, black squares) and of D' to G (D'/G, blue circles).

The calculation with the 6-311+G(d,p) basis set showed that the Raman spectrum of monomer **1** has three prominent peaks at 2146, 1566, and 1288 cm⁻¹, corresponding to A, G and D modes, respectively (Figure 3a). The A mode is mainly contributions from C≡C stretching (C₁₃ in Figure 3b₁), and the G mode mostly comes from C=C aromatic stretching (C₁₂ in Figure b₁), while the stretching of the C-C bonds (C₁₁ in Figure 3b₁) between triply-coordinated atoms and its doubly-coordinated neighbors make the largest contribution to the D mode. Once the homocoupling reaction occurs, a sharp peak at 2241 cm⁻¹ (A' mode) appears, which is attributed to the stretching vibration of the conjugated diyne groups; *i.e.*, synchronous stretching of two adjacent acetylene bonds (C₂₃ in Figure 3b₂). In contrast, the stretching of the bonds between two carbon triple bonds (C₂₂ in Figure 3b₂) coupled with that of the C-C bonds between triply-coordinated atoms and its doubly-coordinated neighbors (C₂₁ in Figure 3b₂) contributed to the new vibrational D' mode (Figure 3a and 3b₂). The peak intensities of the A, A', G, and D' modes gradually increase with polymerization degree *n* (see Figure S4 in the Supporting Information), but the peak positions shift in different directions. The frequencies of the A and A' modes remain constant because the vibrations tend to be localized near the triple carbon bonds. The G vibration changes little, except for in the

Raman spectrum of compound **4**, which shows a shoulder peak at 1552 cm⁻¹ mainly from the extended C=C bonds of the central phenyl rings. However, the frequency of the D' vibration exhibits a blue shift from 1433 to 1435 to 1440 cm⁻¹ for compounds **2**, **3**, and **4** with increasing *n*.

To better understand the variation of the Raman spectra with polymerization degree for the systems based on **1**, we calculated the Raman spectra of more oligomers (compounds **1–4**, **4b**, **6**, **6b**, **12**) using the smaller 6-31G(d) basis set (Figure 3c). Although the Raman peak positions calculated with the 6-31G(d) basis set are not as accurate as those determined with the 6-311+G(d,p) basis set, the variation trends of both Raman peak position and intensity with *n* are consistent for both basis sets (see Table S2 and Figure S4 in the Supporting Information). As shown in Figure S4, the peak intensities of the A, A', G, and D' modes increase monotonically with *n* for the systems we examined. In particular, the intensity ratio of A' to A (A'/A) linearly increases with *n*, while the ratio of D' to G (D'/G) starts to converge at large *n* (Figure 3d). The Raman peak positions of A' and A are constant, as discussed above, while those of G and D' depend on both the degree and direction of polymerization (Figure 3c). The changes of the Raman peak positions gradually decrease with increasing *n*. For example, the Raman peak positions of the G mode are the same for molecules **6** and **12** and those of the D' mode differ by only 2 cm⁻¹. The oligomers showed more vibration modes in the range from 1200 to 1400 cm⁻¹, but the intensities are relatively low.

3.3 Raman spectra of 2D materials

Based on the above analyses, we attempted to predict the Raman spectrum of 2D TEb sheets using a recursive method⁴⁶ and rationalizing the vibrational modes. The A' and A vibrations are characteristic of alkynes. The A' mode is mostly attributed to the stretching vibration of the conjugated diyne groups and shows strong Raman activity at 2241 cm⁻¹ for all of the oligomers, so this peak is also expected to be present in the Raman spectrum of a 2D TEb sheet. In contrast, the A mode mainly comes from the vibration of the ethynyl groups and would not be present in the Raman spectrum of the 2D TEb sheet. This is also consistent with the above observation that A'/A increases with *n* (Figure 3d). The intensity of the G mode indicates the number of phenyl rings, and the peak position is not affected much by the linked groups. Therefore, the 2D TEb sheet is expected to possess a Raman peak near 1560 cm⁻¹ from the G mode. The D' mode is mostly influenced by the stretching of the bonds between two carbon triple bonds (C₂₂ in Figure b₂), which is Raman active because of the molecule's D_{2h} symmetry. Moreover, the ratio of the intensity of D' to G modes (D'/G) tends to converge for TEb oligomers at large *n* (Figure 3d) and the peak position of D' approaches 1444 cm⁻¹. Other Raman peaks were temporarily ignored because they show low Raman activity in oligomers. Overall, the speculated Raman spectrum of the ideal 2D TEb network has three strong

peaks at 2241 (A'), 1560 (G), and 1444 cm⁻¹ (D'), as shown in **Figure 3a**.

Notably, the vibrations of the above speculated Raman peaks (A', G, and D') for 2D TEB (**Figure 3a**) all occur at the Γ point in reciprocal space. The conservation of momentum is satisfied in the Raman response without the involvement of any defects. Thus, these are intrinsic Raman peaks of 2D TEB. This is different from the case of graphene where the ring-breathing mode (D) occurs at the K point and is inhibited without defects (so the D peak in graphene acts as an indicator of the content of defects). However, above speculated peaks in 2D TEB cannot be used to characterize defect content. Graphdiyne may possess similar Raman features to 2D TEB.

3.4 Combination of Raman and IR spectroscopies

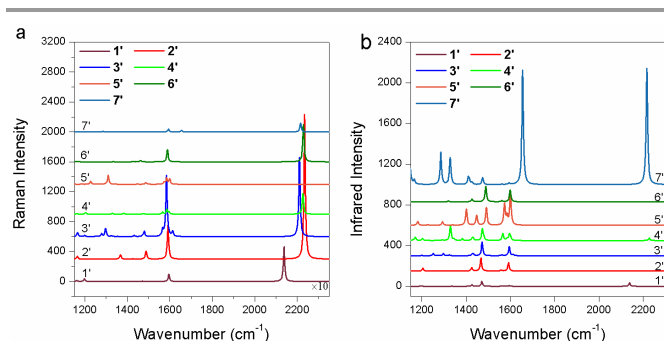


Figure 4. Calculated (a) Raman and (b) IR spectra for molecules 1'–7'. The Raman intensity of molecule 1' was amplified 10 times.

Besides the homocoupling products, many side reactions could also occur in the systems of **1** and **1'**. To differentiate the various functional groups, we calculated the Raman spectra of compounds 1'–7' (**Figure 4a**). The most obvious change in the Raman spectrum of **1'** after homocoupling is the appearance of the strong Raman-active vibration A', which is similar to that of TEB. Unexpectedly, the byproducts also have Raman peaks around 2220 cm⁻¹ except for compound **5'**. The relative Raman positions of the C≡C stretching peak for compounds **3'**, **4'**, **6'**, and **7'** compared with the corresponding peak of **2'** are -27, -9, -5, and -20 cm⁻¹, respectively. The aromatic ring stretching peak also shows Raman activity for all of the products, and the largest difference between the peak position of the byproducts and the corresponding peak of **2'** is -8 cm⁻¹. Although the D' vibration is unique for the homocoupling products, another peak exists near its Raman peak for compound **3'**. In addition, compounds **3'** and **5'** both have a coupled C–H vibration and ring breathing peak at 1298 and 1310 cm⁻¹, respectively, which is not present in the other compounds. Byproduct **7'** also has a unique C=O stretching vibration at 1656 cm⁻¹, although its Raman intensity is very low so it is difficult to detect. Overall, the functional groups of compounds **4'**, **6'**, and **7'** are difficult to distinguish in Raman spectra, whereas the functional groups of compounds **3'** and **5'** are relatively easy to distinguish.

Because it is difficult to use Raman spectroscopy to identify all of the functional groups introduced by the side reactions, we also used IR spectroscopy to examine the systems, which also

shows molecular vibrations but usually provides complementary information to Raman spectroscopy. The calculated results are summarized in **Figure 4b**. Compound **7'** is the easiest to identify because of the strong IR activity of the C=O stretching peak at 1655 cm⁻¹ and C≡C stretching peak at 2216 cm⁻¹. If the analogues of **7'** are ruled out in the system, the similar structures of **4'** and **5'** can be confirmed by their IR peaks near 1330 and 1401 cm⁻¹, respectively. The IR spectra of **6'** and **2'** show similar peak shape, but the former has a peak at 1467 cm⁻¹ while the latter has one at 1489 cm⁻¹. Products **2'** and **3'** cannot be differentiated from IR spectra alone. However, we can identify almost all of the types of byproducts by combining Raman and IR spectroscopies.

3.5 Structural analysis of experimental sample

The insights obtained from the calculations are useful for analyzing experimental results. **Figure 5a** shows a typical Raman spectrum of the product synthesized using monomer **1** as the reactant. The disappearance of the peak at ~2100 cm⁻¹ indicates that **1** has reacted. The two peaks at 1398 and 1431 cm⁻¹ are consistent with the calculated Raman peaks of oligomers of **1**, but it is also possible that they belong to large variety of saturated hydrocarbons. The peaks at 2223 and 2191 cm⁻¹ suggest the formation of both the targeted product and byproducts. Because the position difference of the two peaks near 2200 cm⁻¹ is greater than 30 cm⁻¹, the functional groups of molecule **3'** might exist in the product. However, we did not observe a peak near 1310 cm⁻¹, which characterizes the formation of molecule **3'**, because of the fluctuation of the baseline. This also leads to difficulty in identifying other byproducts. Generally, a carbon material with amorphous structure displays much broader Raman peaks compared with that of a crystalline sample. In **Figure 5a**, the peaks are sharp, suggesting little or no amorphous structure formed. Interestingly, by analyzing the Raman spectra obtained for our synthesized films and reported in the literature,²⁹ we did not observe any high-order (multiphonon) Raman peaks as found for graphene,⁴⁷ which may suggest that high-order Raman resonant processes are not important in 2D TEB and other sp–sp² carbon materials. We also measured the IR spectra of the sample (**Figure 5b**). Two strong IR peaks at ~1704 and ~2215 cm⁻¹ indicate that

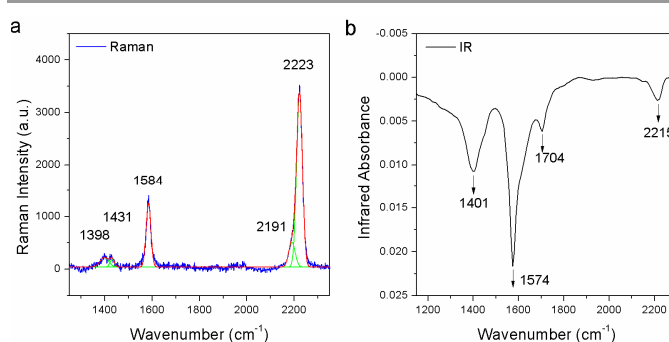


Figure 5. (a) Raman and (b) IR spectra of a typical experimental sample. Raman spectra are fitted by five Gaussian functions after baseline correction.

maybe there exist some analogue of compound 7'. The peaks near 1574 and 1401 cm^{-1} are broad and the superimposition of multiple peaks, indicating a similar structure to 5'. Although it is currently difficult to identify the structures present in the experimental sample, the calculation analysis provides criteria to identify the degree of polymerization and functional groups in sp-sp^2 carbon materials.

4. Conclusions

In summary, we used Raman and IR spectroscopies to identify the structure of sp-sp^2 carbon materials. After demonstrating that many coupling reactions of alkynes can occur spontaneously at room temperature, we conducted a combined computational and experimental study of the vibration spectra of several alkynes. Regular changes of the Raman spectra were observed with increasing homocoupling polymerization degree. The three Raman-active modes, A' ($\sim 2240 \text{ cm}^{-1}$), G ($\sim 1565 \text{ cm}^{-1}$), and D' ($\sim 1440 \text{ cm}^{-1}$), were found to be important for identifying the degree of polymerization. By rationalizing the vibrational modes of various oligomers, we predicted the Raman spectrum of the 2D-TEB network. The combination of Raman and IR spectra is useful for identifying the functional groups in sp-sp^2 carbon materials. Based on this, we examined the structure of an experimental sample.

Acknowledgements

We thank Shibin Deng and Zhenzhu Li for valuable discussion. This work was supported by the National Natural Science Foundation of China (Grant No. 21373015, 51121091, and 51290272), the Ministry of Science and Technology of China (Grant No. 2013CB932603, 2012CB933404, and 2011CB933003), and the Overseas and Hong Kong, Macao Young Scholars Collaborative Research Fund (Grant No. 21129001).

Notes and references

Center for Nanochemistry, College of Chemistry and Molecular Engineering, Peking University, Beijing 100871, PR China
E-mail: zfliu@pku.edu.cn, jinzhang@pku.edu.cn,
LiuZhiRong@pku.edu.cn

^aThese authors contributed equally to this work.

Electronic Supplementary Information (ESI) available: theoretical and experimental methods, test calculations, and the Raman intensity of TEB oligomers. See DOI: 10.1039/b000000x/

- R. B. Heimann, S. E. Evsyukov and Y. Koga, *Carbon*, 1997, **35**, 1654-1658.
- K. S. Novoselov, A. K. Geim, S. V. Morozov, D. Jiang, Y. Zhang, S. V. Dubonos, I. V. Grigorieva and A. A. Firsov, *Science*, 2004, **306**, 666-669.
- A. Hirsch, *Nat Mater*, 2010, **9**, 868-871.
- A. N. Enyashin and A. L. Ivanovskii, *Phys Status Solidi B*, 2011, **248**, 1879-1883.
- J. Y. Wang, H. Q. Huang, W. H. Duan and Z. R. Liu, *J Chem Phys*, 2013, **139**, 184701.
- X.-L. Sheng, Q.-B. Yan, F. Ye, Q.-R. Zheng and G. Su, *Phys Rev Lett*, 2011, **106**, 155703.
- S. Nardecchia, D. Carriazo, M. L. Ferrer, M. C. Gutierrez and F. del Monte, *Chem Soc Rev*, 2013, **42**, 794-830.
- Z. R. Liu, J. Y. Wang and J. L. Li, *Phys Chem Chem Phys*, 2013, **15**, 18855-18862.
- R. H. Baughman, H. Eckhardt and M. Kertesz, *J Chem Phys*, 1987, **87**, 6687-6699.
- A. L. Ivanovskii, *Prog Solid State Ch*, 2013, **41**, 1-19.
- N. Narita, S. Nagai, S. Suzuki and K. Nakao, *Phys Rev B*, 1998, **58**, 11009-11014.
- D. Malko, C. Neiss, F. Vines and A. Gorling, *Phys Rev Lett*, 2012, **108**, 086804.
- S. W. Cranford and M. J. Buehler, *Carbon*, 2011, **49**, 4111-4121.
- J. Kang, J. B. Li, F. M. Wu, S. S. Li and J. B. Xia, *J Phys Chem C*, 2011, **115**, 20466-20470.
- Y. Y. Zhang, Q. X. Pei and C. M. Wang, *Appl Phys Lett*, 2012, **101**, 081909.
- H. Q. Huang, W. H. Duan and Z. R. Liu, *New J Phys*, 2013, **15**, 023004.
- Y. Jiao, A. Du, M. Hankel, Z. Zhu, V. Rudolph and S. C. Smith, *Chem Commun*, 2011, **47**, 11843-11845.
- S. W. Cranford and M. J. Buehler, *Nanoscale*, 2012, **4**, 4587-4593.
- H. Y. Zhang, X. J. He, M. W. Zhao, M. Zhang, L. X. Zhao, X. J. Feng and Y. H. Luo, *J Phys Chem C*, 2012, **116**, 16634-16638.
- Y. H. Guo, K. Jiang, B. Xu, Y. D. Xia, J. Yin and Z. G. Liu, *J Phys Chem C*, 2012, **116**, 13837-13841.
- H. J. Hwang, J. Koo, M. Park, N. Park, Y. Kwon and H. Lee, *The Journal of Physical Chemistry C*, 2013, **117**, 6919-6923.
- H. Y. Zhang, Y. Y. Xia, H. X. Bu, X. P. Wang, M. Zhang, Y. H. Luo and M. W. Zhao, *J Appl Phys*, 2013, **113**.
- N. L. Yang, Y. Y. Liu, H. Wen, Z. Y. Tang, H. J. Zhao, Y. L. Li and D. Wang, *Acs Nano*, 2013, **7**, 1504-1512.
- S. Wang, L. Yi, J. E. Halpert, X. Lai, Y. Liu, H. Cao, R. Yu, D. Wang and Y. Li, *Small*, 2012, **8**, 265-271.
- H. Du, Z. Deng, Z. Lü, Y. Yin, L. Yu, H. Wu, Z. Chen, Y. Zou, Y. Wang, H. Liu and Y. Li, *Synthetic Metals*, 2011, **161**, 2055-2057.
- M. M. Haley, *Pure Appl Chem*, 2008, **80**, 519-532.
- J. Sakamoto, J. van Heijst, O. Lukin and A. D. Schluter, *Angew Chem Int Edit*, 2009, **48**, 1030-1069.
- F. Diederich and M. Kivala, *Adv Mater*, 2010, **22**, 803-812.
- G. X. Li, Y. L. Li, H. B. Liu, Y. B. Guo, Y. J. Li and D. B. Zhu, *Chem Commun*, 2010, **46**, 3256-3258.
- Y. Q. Zhang, N. Kepcija, M. Kleinschrodt, K. Diller, S. Fischer, A. C. Papageorgiou, F. Allegretti, J. Bjork, S. Klyatskaya, F. Klappenberger, M. Ruben and J. V. Barth, *Nat Commun*, 2012, **3**, 1286.

31. J. Eichhorn, W. M. Heckl and M. Lackinger, *Chem Commun*, 2013, **49**, 2900-2902.
32. H.-Y. Gao, J.-H. Franke, H. Wagner, D. Zhong, P.-A. Held, A. Studer and H. Fuchs, *J. Phys. Chem. C*, 2013, **117**, 18595-18602.
33. H.-Y. Gao, H. Wagner, D. Y. Zhong, J.-H. Franke, A. Studer and H. Fuchs, *Angew Chem Int Edit*, 2013, **52**, 4024-4028.
34. A. C. Ferrari and J. Robertson, eds., *Raman Spectroscopy in Carbons: from Nanotubes to Diamond*, 2004.
35. E. Fuente, J. A. Menéndez, M. A. Díez, D. Suárez and M. A. Montes-Morán, *The J. Phys. Chem.B*, 2003, **107**, 6350-6359.
36. A. C. Ferrari, J. C. Meyer, V. Scardaci, C. Casiraghi, M. Lazzeri, F. Mauri, S. Piscanec, D. Jiang, K. S. Novoselov, S. Roth and A. K. Geim, *Phys Rev Lett*, 2006, **97**, 187401.
37. L. M. Malard, M. A. Pimenta, G. Dresselhaus and M. S. Dresselhaus, *Physics Reports*, 2009, **473**, 51-87.
38. A. Jorio, R. Saito, J. H. Hafner, C. M. Lieber, M. Hunter, T. McClure, G. Dresselhaus and M. S. Dresselhaus, *Phys Rev Lett*, 2001, **86**, 1118-1121.
39. R. D. Gaussian 03, G. W. T. M. J. Frisch, H. B. Schlegel, G. E. Scuseria, J. R. C. M. A. Robb, J. A. Montgomery, Jr., T. Vreven, J. C. B. K. N. Kudin, J. M. Millam, S. S. Iyengar, J. Tomasi, B. M. V. Barone, M. Cossi, G. Scalmani, N. Rega, H. N. G. A. Petersson, M. Hada, M. Ehara, K. Toyota, J. H. R. Fukuda, M. Ishida, T. Nakajima, Y. Honda, O. Kitao, M. K. H. Nakai, X. Li, J. E. Knox, H. P. Hratchian, J. B. Cross, C. A. V. Bakken, J. Jaramillo, R. Gomperts, R. E. Stratmann, A. J. A. O. Yazyev, R. Cammi, C. Pomelli, J. W. Ochterski, K. M. P. Y. Ayala, G. A. Voth, P. Salvador, J. J. Dannenberg, S. D. V. G. Zakrzewski, A. D. Daniels, M. C. Strain, D. K. M. O. Farkas, A. D. Rabuck, K. Raghavachari, J. V. O. J. B. Foresman, Q. Cui, A. G. Baboul, S. Clifford, B. B. S. J. Cioslowski, G. Liu, A. Liashenko, P. Piskorz, R. L. M. I. Komaromi, D. J. Fox, T. Keith, M. A. Al-Laham, A. N. C. Y. Peng, M. Challacombe, P. M. W. Gill, W. C. B. Johnson, M. W. Wong, C. Gonzalez, and J. A. Pople, and I. Gaussian, Wallingford CT, 2004.
40. X. Xu and W. A. Goddard, *J Chem Phys*, 2004, **121**, 4068-4082.
41. M. H. Jamróz, *Vibrational Energy Distribution Analysis VEDA 4*, Warsaw, 2004.
42. M. H. Jamróz, *Spectrochimica Acta Part A: Molecular and Biomolecular Spectroscopy*, 2013, **114**, 220-230.
43. S. Ostrowski, M. H. Jamroz, J. E. Rode and J. C. Dobrowolski, *The journal of physical chemistry. A*, 2012, **116**, 631-643.
44. J. R. Maia, J. A. Lima Jr, P. T. C. Freire, J. Mendes Filho, C. E. S. Nogueira, A. M. R. Teixeira, A. S. de Menezes, C. M. R. Remédios and L. P. Cardoso, *Journal of Molecular Structure*, 2013, **1054-1055**, 143-149.
45. P. Sutter, M. S. Hybertsen, J. T. Sadowski and E. Sutter, *Nano Letters*, 2009, **9**, 2654-2660.
46. C. Castiglioni, F. Negri, M. Rigolio and G. Zerbi, *The Journal of Chemical Physics*, 2001, **115**, 3769-3778.
47. D. M. Basko, *Phys Rev B*, 2008, **78**, 125418.